This article has been accepted for publication in a future issue of this journal, but has not been fully edited. Content may change prior to final publication. Citation information: DOI 10.1109/TIE.2015.2477484, IEEE Transactions on Industrial Electronics

Discrete-Time Repetitive Control of Flyback CCM Inverter for PV Power Applications

Sung-Ho Lee, Woo-Jun Cha, Bong-Hwan Kwon, *Member, IEEE,* and Minsung Kim, *Member, IEEE*

***Abstract*—In this paper, a discrete-time repetitive controller (RC) is proposed for flyback inverter operating in continuous conduction mode, which has simple structure, low cost, and high efficiency. Conventional controller results in poor control performance due to the effect of the right-half-plane zero in CCM operation. To achieve the accurate tracking performance and disturbance rejection, the repetitive controller is developed and applied to flyback inverter in CCM operation. In the RC scheme, a low-pass filter is used to allow tracking and rejection of periodic signals within a specified frequency range. A phase lead compensator is also used to compensate for the system delay caused by digital implementation. The stability of the closed-loop system is derived and the zero tracking error is achieved. Numerical simulations validated the proposed control approach, and experimental tests using a 200-W digitally-controlled module integrated converter prototype confirmed its feasibility.**

***Index Terms*—Module-integrated converter, right-half-plane zero, low-pass filter, phase-lead compensation.**

I. Introduction

RECENTLY, an AC photovoltaic (PV) module system has been of interest as a trend for future PV power systems [1, 2]. Unlike conventional centralized PV systems, the AC PV module system provides independent operation for each individual PV module; this design allows all modules to operate at their maximum power point (MPP) and reduces power losses caused by PV module mismatch and partial shading [3, 4]. Moreover, the AC PV module system is more reliable and easier to maintain than are centralized PV systems [5].

In the AC PV module system, a module-integrated converter (MIC) is attached to a single PV panel to ensure maximum power extract and to provide the power to the utility grid. The acceptability of the MIC is evaluated by conversion efficiency, harmonic of output current, cost, and reliability. To meet these requirements, a single-stage flyback inverter topology with an unfolding circuit has been widely used due to its small number of components and its potential for high efficiency and reliability [6, 7].

Operation modes of the flyback inverter can be classified into discontinuous conduction mode (DCM) and continuous conduction mode (CCM). In flyback inverters that operate under DCM [3], [8–10], the transfer function from control input to output current is a constant; thus, the output current control can be controlled easily and simply. However, the flyback inverter in DCM imposes high current stress on devices; it results in decrease of conversion efficiency. In addition, the filter design becomes difficult due to the high current ripple. Compared to the DCM flyback inverters, the CCM flyback inverter has many advantages such as higher efficiency with lower current stress, easier filter design, and lower electromagnetic interference (EMI). However, in a CCM flyback inverter, the transfer function from control input to output current has a right-half-plane (RHP) zero which destabilizes the feedback control loop [11]. Moreover, the RHP zero location depends on the operating point, which varies in a wide range in the case of PV MIC applications. Thus, the controller should accommodate the minimum RHP zero; this requirement causes the degradation of the controller bandwidth and difficulty in controlling the output current [12]. This characteristic limits the use of CCM flyback inverters in practice despite their numerous merits.

To avoid this problem, some studies [11–13] used feedback control of the primary current; this approach is an open-loop control of the output current. In this case, the control approach bypasses the difficulties posed by the RHP zero. However, total harmonic distortion (THD) of the output current is high, because this approach controls the output current indirectly.

The repetitive controller is widely used as an effective solution to track a periodic signal and to eliminate periodic disturbance in dynamic systems [14–16]. In the repetitive control scheme, the present control input is obtained using knowledge obtained in the previous period, and this operation is performed repetitively. Hence, the repetitive controller generates the control input that ensures zero tracking error [19].

In this paper, the feedback of the output current and the use of repetitive control algorithm are proposed for a flyback inverter that operates in CCM. This direct control of the output current can ensure the stability of a closed-loop system more clearly, and does not need the additional sensor to measure the primary current. The conventional controller, which consists of a linear controller and a feedforward controller, results in poor control accuracy due to the RHP zero which limits the available controller bandwidth. To ensure good tracking ability and disturbance rejection, the repetitive controller is

Manuscript received January 28, 2015; revised May 4, 2015 and June 16, 2015; accepted June 17, 2015.

Copyright © 2015 IEEE. Personal use of this material is permitted. However, permission to use this material for any other purposes must be obtained from the IEEE by sending a request to pubs-permissions@ieee.org.

This research was supported by the MSIP (Ministry of Science, ICT and Future Planning), Korea, under the "ICT Consilience Creative Program" (IITP-2015-R0346-15-1007) supervised by the IITP (Institute for Information & communications Technology Promotion)

S.-H. Lee, W.-J. Cha, and B.-H. Kwon are with the Department of Electrical Engineering, Pohang University of Science and Technology (POSTECH), Pohang, 790-784, Korea (e-mail: mulem@postech.ac.kr; woo-jun79@postech.ac.kr; bhkwon@postech.ac.kr).

M.S. Kim is with the Department of Creative IT Engineering, Pohang University of Science and Technology (POSTECH), Pohang, 790-784, Korea (e-mail: redtoss@postech.ac.kr).

0278-0046 (c) 2015 IEEE. Personal use is permitted, but republication/redistribution requires IEEE permission. See http://www.ieee.org/publications_standards/publications/rights/index.html for more information.

This article has been accepted for publication in a future issue of this journal, but has not been fully edited. Content may change prior to final publication. Citation information: DOI 10.1109/TIE.2015.2477484, IEEE Transactions on Industrial Electronics

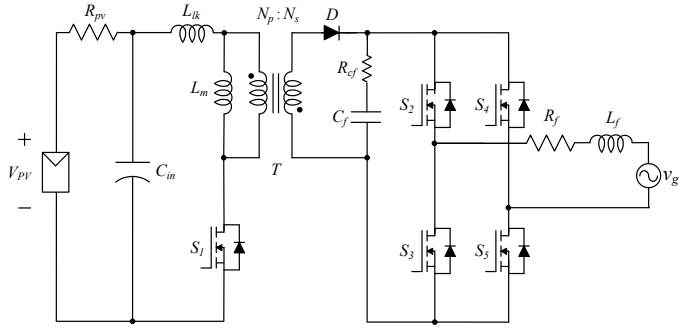

Fig. 1. The circuit diagram of flyback inverter.

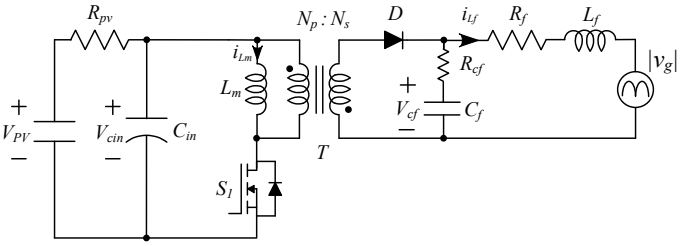

Fig. 2. The equivalent circuit of flyback inverter.

developed. In the repetitive control scheme, a low-pass filter is used to disable the learning at high-frequency so that it allows tracking/rejecting periodic signals within a specified frequency range. A phase lead compensator is also used to compensate for system delay that is caused by digital implementation. The stability of the closed-loop system is derived and the zero tracking error is achieved. Simulation and experimental results verify the effectiveness of the proposed control scheme.

This paper is organized as follows. In Section 2, the inverter modelling is presented. In Section 3, the proposed controller is presented and the stability of the closed-loop system is derived. In Section 4, experimental setup is presented. The simulation and experimental results are shown in Section 5. Finally, conclusion is drawn in Section 6.

II. Problem Formulation and Preliminary

A. Averaged model of flyback inverter in CCM operation

The circuit diagram of the flyback inverter is shown in Fig. 1. The PV current is drawn from the PV panel and modulated to a full wave rectified sinusoidal waveform by high frequency switching. The unfolding H-bridge unfolds the rectified sinusoidal current and injects the resulting sinusoidal ac current into the grid. The capacitor-inductor filter reduces the harmonic components in the ac current.

Fig. 2 shows the equivalent circuit of flyback inverter. Denoting $\mathbf{x}(t) = [i_{L_m}(t),\ v_{C_{in}}(t), i_{L_f}(t), v_{C_f}(t)]^T$, $\mathbf{v}(t) = [V_{pv}(t), |v_g(t)|]^T$, $\mathbf{y}(t) = i_{L_f}(t)$, the state-space equations in the turn-on and turn-off subintervals are expressed in the following equations, respectively.

During turn-on subinterval:

$$\dot{\mathbf{x}}(t) = \begin{bmatrix} 0 & \frac{1}{L_m} & 0 & 0 \\ -\frac{1}{C_{in}} & -\frac{1}{R_{pv}C_{in}} & 0 & 0 \\ 0 & 0 & -\frac{R_{C_f}+R_f}{L_f} & \frac{1}{L_f} \\ 0 & 0 & -\frac{1}{C_f} & 0 \end{bmatrix} \mathbf{x}(t) + \begin{bmatrix} 0 & 0 \\ \frac{1}{R_{pv}C_{in}} & 0 \\ 0 & -\frac{1}{L_f} \\ 0 & 0 \end{bmatrix} \mathbf{v}(t), \quad (1)$$

$$\mathbf{y}(t) = \begin{bmatrix} 0 & 0 & 1 & 0 \end{bmatrix} \mathbf{x}(t), \quad (2)$$

During turn-off subinterval:

$$\dot{\mathbf{x}}(t) = \begin{bmatrix} -\frac{R_{C_f}}{n^2L_m} & 0 & \frac{R_{C_f}}{nL_m} & -\frac{1}{nL_m} \\ 0 & -\frac{1}{R_{pv}C_{in}} & 0 & 0 \\ \frac{R_{C_f}}{nL_f} & 0 & -\frac{R_{C_f}+R_f}{L_f} & \frac{1}{L_f} \\ \frac{1}{nC_f} & 0 & -\frac{1}{C_f} & 0 \end{bmatrix} \mathbf{x}(t) + \begin{bmatrix} 0 & 0 \\ \frac{1}{R_{pv}C_{in}} & 0 \\ 0 & -\frac{1}{L_f} \\ 0 & 0 \end{bmatrix} \mathbf{v}(t), \quad (3)$$

$$\mathbf{y}(t) = \begin{bmatrix} 0 & 0 & 1 & 0 \end{bmatrix} \mathbf{x}(t), \quad (4)$$

where i_{L_m} is the current through the magnetazing inductor, $v_{C_{in}}$ is voltage across the capacitor, i_{L_f} is the current through the output inductor, v_{C_f} is the voltage across the output capacitor. n is the secondary to primary turns ratio of the transformer.

Combining (1)−(4) using the state-space averaging method, the averaged model can be developed as in [1]

$$\dot{\mathbf{x}}(t) = \begin{bmatrix} -\frac{R_{c_f}}{n^2L_m} & 0 & \frac{R_{c_f}}{nL_m} & -\frac{1}{nL_m} \\ 0 & -\frac{1}{R_{pv}C_{in}} & 0 & 0 \\ \frac{R_{c_f}}{nL_f} & 0 & -\frac{R_{C_f}+R_f}{L_f} & \frac{1}{L_f} \\ \frac{1}{nC_f} & 0 & -\frac{1}{C_f} & 0 \end{bmatrix} \mathbf{x}(t) + \begin{bmatrix} \frac{R_{C_f}}{n^2L_m} i_{L_m} + \frac{1}{L_m} v_{C_{in}} - \frac{R_{C_f}}{nL_m} i_{L_f} + \frac{1}{nL_m} v_{C_f} \\ -\frac{1}{C_{in}} i_{L_m} \\ -\frac{R_{C_f}}{nL_f} i_{L_m} \\ -\frac{1}{nC_f} i_{L_m} \end{bmatrix} \cdot D_c(t) + \begin{bmatrix} 0 & 0 \\ \frac{1}{R_{pv}C_{in}} & 0 \\ 0 & -\frac{1}{L_f} \\ 0 & 0 \end{bmatrix} \mathbf{v}(t), \quad (5)$$

$$\mathbf{y}(t) = \begin{bmatrix} 0 & 0 & 1 & 0 \end{bmatrix} \mathbf{x}(t), \quad (6)$$

where $D_c(t)$ is the control duty cycle.

B. Problem formulation

By linearizing the averaged model, the small signal model can be derived as follows:

0278-0046 (c) 2015 IEEE. Personal use is permitted, but republication/redistribution requires IEEE permission. See http://www.ieee.org/publications_standards/publications/rights/index.html for more information.

This article has been accepted for publication in a future issue of this journal, but has not been fully edited. Content may change prior to final publication. Citation information: DOI 10.1109/TIE.2015.2477484, IEEE Transactions on Industrial Electronics

$$G_{id}(s) = \frac{\tilde{i}_{L_f}(s)}{\tilde{d}(s)} = \frac{a_1 s^3 + a_2 s^2 + a_3 s + a_4}{s^4 + b_1 s^3 + b_2 s^2 + b_3 s + b_4}, \quad (7)$$

where $\tilde{i}_{L_f}(t)$ and $\tilde{d}(t)$ are the small ac variations of $i_{L_f}(t)$ and $D_c(t)$. The parameters a_j and b_j for all $j = 1, ..., 4$ are defined in the Appendix A. By analyzing the small signal model, the system has one RHP zero, two left-half-plane (LHP) zero, and four LHP poles.

In the following section, the controller will be developed in discrete-time domain. To get a better connection between the flyback inverter system and the controller, the small signal model needs to be represented as the discrete-time transfer function. Using backward difference method with sampling period of T_s, it can be described as:

$$G_{id}(z) = \frac{e_1 z^4 + e_2 z^3 + e_3 z^2 + e_4 z}{z^4 + f_1 z^3 + f_2 z^2 + f_3 z + f_4}, \quad (8)$$

where the parameters e_j and f_j for all $j = 1, ..., 4$ are defined in the Appendix A.

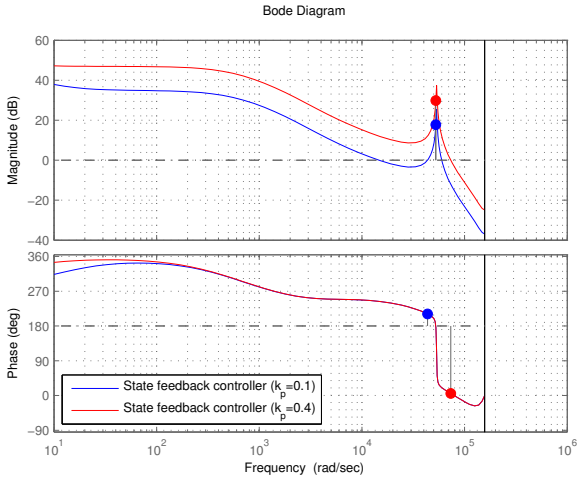

Fig. 3. The Bode plot of compensated system when the state-feedback controller is used (blue); when the high-gain state-feedback controller is used (red). The dot in each magnitude Bode plot denotes the gain margin of the compensated system. The dot in each phase Bode plot denotes the phase margin of the compensated system.

III. Controller Design

A. Conventional controller

The operating condition of the flyback inverter in CCM changes slowly during a grid period compared to a switching period; the flyback inverter can be assumed to operate in quasi-steady state in each instant of the grid period. By assuming quasi steady-state operation and using volt-second balance for the magnetizing inductance L_m over one switching period T_s, the nominal duty ratio $D_n(t)$ for flyback inverter in CCM can be obtained as [1]

$$D_n(t) = \frac{|v_g(t)|}{|v_g(t)| + nV_{pv}(t)}. \quad (9)$$

Even though $D_n(t)$ does not directly determine the output current, the use of the nominal duty helps the flyback inverter in CCM to generate the desired output current by alleviating the effect of the disturbances. Thus, it reduces the burden on the state-feedback controller, and so makes the overall control system easily achieve the fast response.

Since $D_n(t)$ has been used to generate the desired output current by alleviating the effect of disturbances such as the grid voltage, a state feedback controller can be utilized to improve the control quality with suppressing the remaining disturbances. The transfer function of a state feedback controller is represented as

$$C_{fb}(z) = k_p + k_i \frac{T_s}{1 - z^{-1}}, \quad (10)$$

where k_p is the proportional controller gain, k_i is the integral controller gain.

However, in flyback inverter under the operating mode of CCM, the nominal duty plus the state feedback controller cannot satisfy the desired control performance, because the transfer function of the flyback inverter in CCM operation has a RHP zero, which was obtained from small signal model (7). In this conventional control scheme, the RHP zero limits the available controller bandwidth. Moreover, the controller should accommodate the minimum RHP zero; it causes the degradation of the available controller bandwidth and so difficulty in controlling the output current.

Fig. 3 shows the Bode plot of the compensated system when the state-feedback controller is used. Used parameters are listed in Table I. As shown in Fig. 3, the RHP zero creates a negative phase shift between 20 and 1kHz so that it reduces the phase margin of the system. In this condition, to ensure the tracking performance and disturbance rejection such as the grid voltage, the high-gain state-feedback controller can be used. However, it increases the system gain at all frequencies and so it reduces the phase margin even more. As a result, it would make the flyback inverter in CCM which has the RHP zero become unstable. To overcome this problem, the repetitive controller is developed in the sequel.

B. Repetitive controller with low-pass filter

The repetitive controller handles systems that performs the same task repetitively. In repetitive control scheme, the knowledge obtained from the previous trial is used to improve the control input for the next trial. Hence, the control input in each trial is adjusted using the tracking error signals obtained from the previous trial, and theoretically achieves zero tracking error [14, 15]. The concept of repetitive controller is shown in Fig. 4.

In the conventional control scheme, the RHP zero limits the available controller bandwidth. To achieve fast dynamical response to input signal at a specific frequency, the repetitive controller is developed. To allow tracking/rejecting periodic signals within a specified frequency range, a low-pass filter is adopted in the repetitive control scheme. Moreover, to compensate for the system delay which comes from digital implementation, the phase lead compensator is used to the repetitive controller scheme.

0278-0046 (c) 2015 IEEE. Personal use is permitted, but republication/redistribution requires IEEE permission. See http://www.ieee.org/publications_standards/publications/rights/index.html for more information.

This article has been accepted for publication in a future issue of this journal, but has not been fully edited. Content may change prior to final publication. Citation information: DOI 10.1109/TIE.2015.2477484, IEEE Transactions on Industrial Electronics

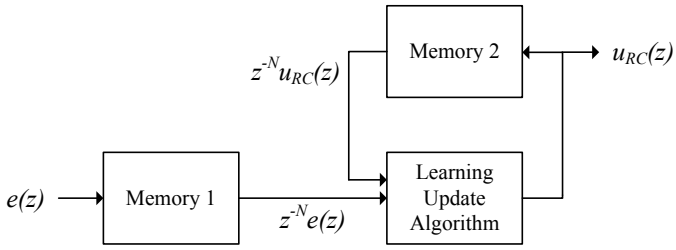

Fig. 4. The concept of repetitive controller.

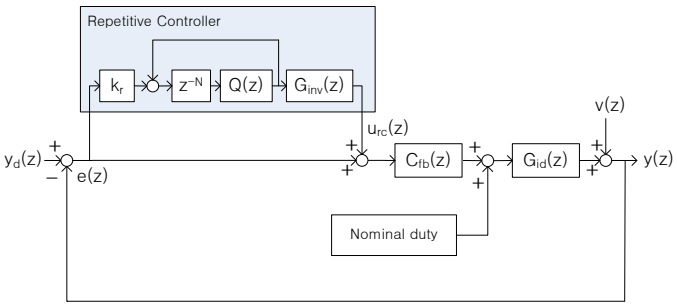

Fig. 5. The schematic diagram of overall control system. $y_d(z)$ is the reference, $e(z)$ is the error, $u_{rc}(z)$ is the repetitive control input, $v(z) = [V_{pv}(z), |v_g(z)|]^T$.

The transfer function of the repetitive controller is

$$C_{rc}(z) = k_r \frac{z^{-N}Q(z)}{1 - z^{-N}Q(z)} G_{inv}(z), \tag{11}$$

where k_r is the repetitive controller gain, $N = f_s/f_g$ with $f_s = 1/T_s$ being the sampling frequency and f_g being the frequency of reference, $Q(z)$ is the low-pass filter, and $G_{inv}(z)$ is the inverse function of the system.

For tracking/rejecting periodic signals within a specified frequency range and easy implementation, $Q(z)$ is chosen as moving average filter with zero phase shift:

$$Q(z) = \Sigma_{i=0}^{p} \alpha_i z^i + \Sigma_{i=1}^{p} \alpha_i z^{-i}, \tag{12}$$

where $\alpha_0 + 2\Sigma_{i=1}^{p}\alpha_i = 1$ with $\alpha_i > 0$, p is the number of samples to be used for filtering. Here, a first order filter $Q(z) = \alpha_1 z + \alpha_0 + \alpha_1 z^{-1}$ is used; as α_0 becomes larger, the cutoff frequency of $Q(z)$ becomes higher.

Due to the system uncertainty, the system delay, and the unknown disturbance, $G_{inv}(z)$ cannot be precisely implemented. Here, to compensate even the effect of the system delay, G_{inv} are set as

$$G_{inv}(z) = z^m. \tag{13}$$

where m is the prediction index.

With the complete repetitive controller, the overall control system is shown in Fig. 5. This control scheme consists of three components: the linear feedback control term that forces the closed-loop system stay within uniform bound; the nominal duty term that generates the desired output current by alleviating the disturbances; the repetitive controller term that enhances the command input response with suppressing the residual disturbances.

Fig. 6 shows the Bode plot of the compensated system when the repetitive controller is used. Used parameters are listed in Table I. The repetitive controller increases the gain around $w_l = 2\pi l f_g$, with $l = 0, 1, 2, ..., L$ without decreasing the phase margin. Thus, it enhances the tracking and disturbance rejection performance. The resonant peak and sharp phase drop at a frequency of 8kHz are introduced by capacitor-inductor filter. It also restricts the controller bandwidth. In grid voltage disturbance, fundamental and low-order harmonic components are dominant. To avoid the control at a high-frequency and suppress fundamental and low-order harmonics components, the low-pass filter is adopted in the repetitive control scheme. It disables the learning at high-frequency. The resulting repetitive controller

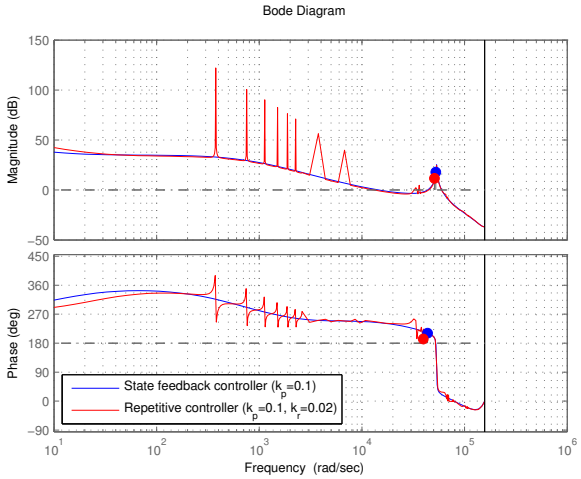

Fig. 6. The Bode plot of compensated system when the state-feedback controller is used (blue); when the repetitive controller with low-pass filter is used (red). The dot in each magnitude Bode plot denotes the gain margin of the compensated system. The dot in each phase Bode plot denotes the phase margin of the compensated system.

amplifies the system gain only within a low frequency region so that it improves the output current tracking performance while suppressing the grid voltage disturbance at a fundamental and low-order harmonic frequencies.

C. Stability analysis

In the repetitive control system shown in Fig. 5, the input-output relationship of the flyback inverter in CCM is described as

$$y(z) = G(z)y_d(z) + S(z)v(z), \tag{14}$$

where $G(z)y_d(z)$ is the command input response and $S(z)v(z)$ is the disturbance response; $G(z)$ is the transfer function from reference to output and $S(z)$ is the sensitivity function; $G(z)$ and $S(z)$ are represented as

$$G(z) = \frac{y(z)}{y_d(z)} = \frac{[1 - Q(z)z^{-N}(1 - k_r z^m)]G_c(z)}{1 - Q(z)z^{-N}(1 - k_r z^m G_c(z))}, \tag{15}$$

$$S(z) = \frac{y(z)}{v(z)} = \frac{[1 - Q(z)z^{-N}](1 - G_c(z))}{1 - Q(z)z^{-N}(1 - k_r z^m G_c(z))}, \tag{16}$$

0278-0046 (c) 2015 IEEE. Personal use is permitted, but republication/redistribution requires IEEE permission. See http://www.ieee.org/publications_standards/publications/rights/index.html for more information.

This article has been accepted for publication in a future issue of this journal, but has not been fully edited. Content may change prior to final publication. Citation information: DOI 10.1109/TIE.2015.2477484, IEEE Transactions on Industrial Electronics

where $G_c(z) = C_{fb}(z)G_{id}(z)/(1 + C_{fb}(z)G_{id}(z))$. Detailed derivations of (15) and (16) are shown in the Appendix B for the sake of completeness.

Defining $w(z) = y_d(z) - v(z)$ and from (15) and (16), the relationship between the error $e(z) = y(z) - y_d(z)$ and the reference $y_d(z)$ and disturbance $v(z)$ can be obtained as

$$\frac{e(z)}{w(z)} = \frac{(1 - Q(z)z^{-N})(1 - G_c(z))}{1 - Q(z)z^{-N}(1 - k_r z^m G_c(z))}, \qquad (17)$$

The transfer function $e(z)/w(z)$ can be written as three systems connected in cascade. The term $1 - Q(z)z^{-N}$ is a low-pass filter and a time delay, and so it is stable. The term $1 - G_c(z)$ which has the same roots as $G_c(z)$. Thus, it can be stable by designing the linear controller. Finally, the term $1 - Q(z)z^{-N}(1 - k_r z^m G_c(z))$ can be described as a positive-feedback closed-loop system with the term $Q(z)z^{-N}(1 - k_r z^m G_c(z))$ in the feedback path. A sufficient condition for the stability of the system with the term $1 - Q(z)z^{-N}(1 - k_r z^m G_c(z))$ is

$$\begin{aligned} &|Q(z)z^{-N}(1 - k_r z^m G_c(z))| \\ &\le |z^{-N}| \cdot |Q(z)(1 - k_r z^m G_c(z))| \\ &\le |Q(z)(1 - k_r z^m G_c(z))| < 1 \\ &\qquad \forall z = e^{jwT_s}, 0 < w < \frac{\pi}{T_s} \end{aligned} \qquad (18)$$

As a result, if the overall control system holds the following stability conditions

1) The closed-loop system $G_c(z)$ without repetitive controller is stable;
2) $|Q(z)(1 - k_r z^m G_c(z))| < 1, \quad \forall z = e^{jwT_s}, 0 < w < \frac{\pi}{T_s}$

then, the system is stable [16, 17]. Moreover, if the frequency of the reference $y_d(t)$ and disturbance $v(t)$ approaches to $w_l = 2\pi l f_g$, with $l = 0, 1, 2, ..., L$ ($L = N/2$ for even N and $L = (N-1)/2$ for odd N), then $z^{-N} = 1$. Assuming $|Q(z)| = 1$ and $\angle Q(z) = 0$, from (15) and (16), we have

$$\lim_{w \to w_l} ||G(z)|| = 1, \qquad \forall w_l \qquad (19)$$

$$\lim_{w \to w_l} ||S(z)|| = 0. \qquad \forall w_l \qquad (20)$$

Equations (19) and (20) indicate that, for any periodic reference and disturbance, a zero steady-state tracking error and disturbance rejection can be guaranteed [19].

IV. Simulation and Experimental Results

To demonstrate the feasibility of the proposed controller, simulation using a simulator Psim and experiment using the prototype were conducted for the flyback inverter operated in CCM. The flyback inverter in CCM was designed for the following specifications: input voltage $V_{pv} = 60\ V$, grid voltage $v_g = 220\ V_{rms}$, and rated output power $P_o = 200\ W$. The major parameters for proposed inverter are listed in Table I. The total system configuration is shown in Fig. 7. The flyback inverter in CCM is controlled by a dsPIC33EP512GM604 digital signal controller. The controller is also implemented with other functions such as phase-locked loop (PLL) and over current protection.

TABLE I
Parameters and Components of the Prototype.

Parameters	Symbols	Value
Nominal voltage of solar panel	V_{pv}	60 V
Grid voltage	v_g	220 V_{rms}
Grid frequency	f_g	60 Hz
Transformer turns ratio	N_p:N_s	14:51
Magnetizing inductance	L_m	50 uH
Leakage inductance	L_{lk}	0.6 uH
Switching frequency	f_s	50 kHz
Resistance	R_{pv}	0.1 Ω
Input capacitance	C_{in}	4.4 mF
Filter inductance	L_f	400 uH
Resistance in filter inductor	R_f	0.24 Ω
Filter capacitance	C_f	1 uF
Resistance in filter capacitor	R_{C_f}	0.1 Ω
Components	**Symbols**	**Part number**
MOSFET	S_1	IPP200N25N3G
Unfolding Switch	$S_2 - S_5$	IPP60R074C6
Transformer core	T	PQ3535
Diode	D	C2D05120A

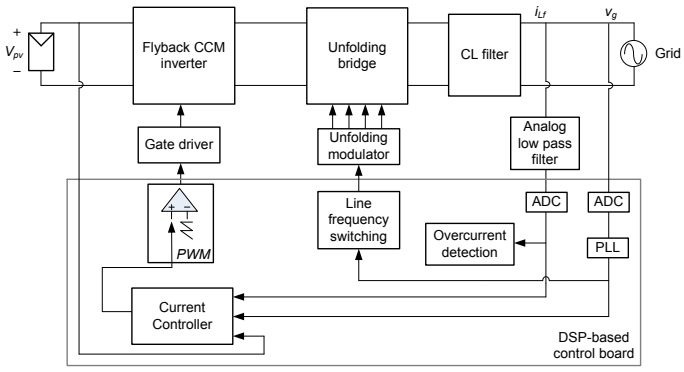

Fig. 7. Configuration of the proposed control system. PWM stands for pulse-width modulation. ADC stands for analog-to-digital converter.

The gains of the state feedback controller (10) and repetitive controller (11) are set as follows: the gains of proportional-integral controller $k_p = 0.1$ and $k_i = 0$, the gain of repetitive controller $k_r = 0.02$, the gains of low-pass filter $\alpha_0 = 0.5$ and $\alpha_1 = 0.25$, the prediction index $m = 1$. The repetitive control gain k_r is chosen to satisfy the convergence condition $|Q(z)(1 - k_r z^m G_c(z)))| < 1$.

A. Simulation results

Fig. 8(a) shows waveforms of the reference and output currents when conventional control scheme with linear controller plus feedforward controller is applied. Linear controller ($k_p = 0.1$) plus feedforward controller is applied for the first 0.05 s. Afterward, linear controller ($k_p = 0.13$) plus feedforward controller is applied. The control scheme shows poor tracking ability due to the effect of RHP zero in CCM operation. Fig. 8(b) shows waveforms of the reference and output current when proposed control scheme is applied. As the learning operation of the proposed controller proceeds, the output current gradually tracks the reference current, and

0278-0046 (c) 2015 IEEE. Personal use is permitted, but republication/redistribution requires IEEE permission. See http://www.ieee.org/publications_standards/publications/rights/index.html for more information.

This article has been accepted for publication in a future issue of this journal, but has not been fully edited. Content may change prior to final publication. Citation information: DOI 10.1109/TIE.2015.2477484, IEEE Transactions on Industrial Electronics

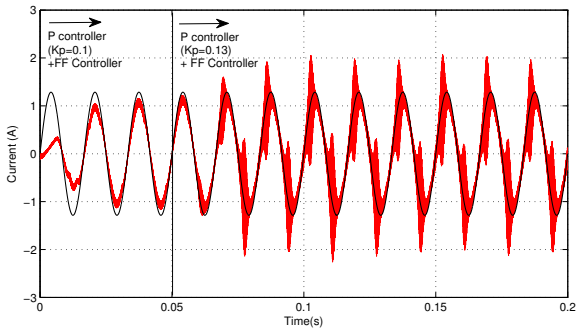

(a)

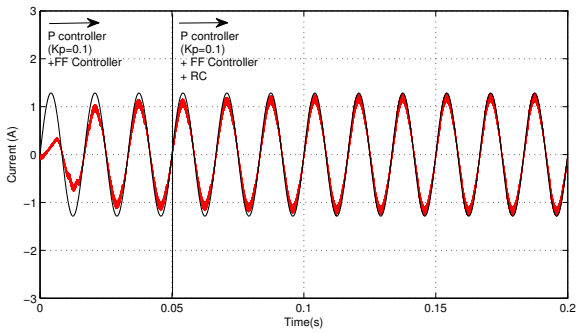

(b)

Fig. 8. The waveforms of desired output current (black) and output current (red). (a) When the conventional controller is used. (b) When the proposed controller is used.

finally the tracking error becomes almost zero.

B. Experimental results

Fig. 9 shows waveforms of the grid voltage v_g and output current i_{L_f} at quarter, half, and full loads conditions when the proposed control scheme is applied. The output current is perfectly sinusoidal and had desired power level. The total harmonic distortion (THD) of the output current is measured less than 2.5% under full load condition. Fig. 10 represents measured efficiency according to load conditions. The maximum efficiency is 96.3%.

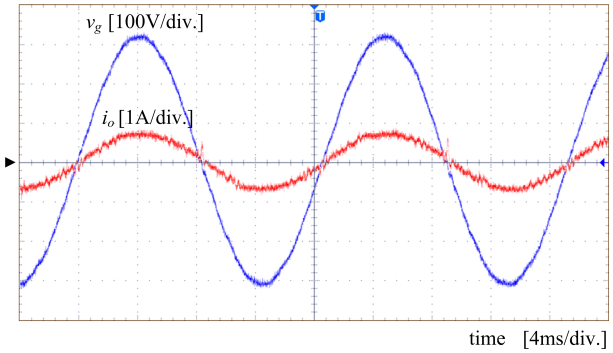

(a)

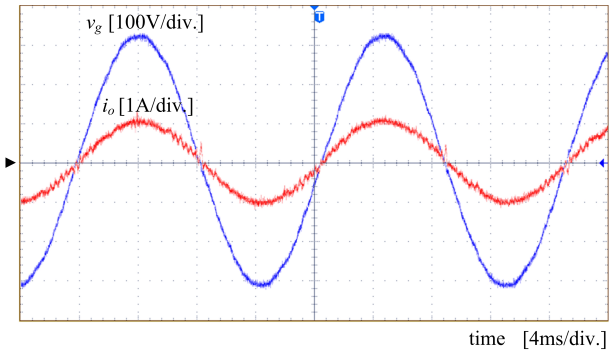

(b)

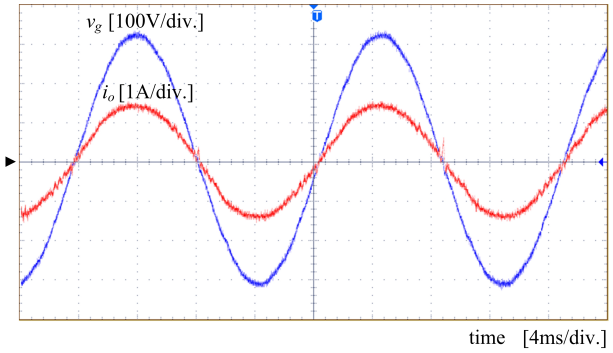

(c)

Fig. 9. The waveforms of grid voltage (purple) and output current (green). (a) Output power $P_o = 50$ W. (b) Output power $P_o = 100$ W. (c) Output power $P_o = 200$ W.

V. Conclusion

In this paper, a repetitive controller is proposed for flyback inverter operating in CCM, which has simple structure, low cost, and high efficiency. Conventional controller results in poor tracking ability due to the effect of RHP zero in CCM operation. To achieve a fast dynamical response, a repetitive controller is developed and applied to the flyback inverter in CCM operation. The low pass filter is adopted to allow tracking/rejecting periodic signals within a specified frequency range. The phase lead compensator is used to compensate for the system delay which comes from digital implementation. The stability of closed-loop system is derived and the zero tracking error is achieved. The effect of RHP zero is analyzed. Comparison of the accuracy of linear controller plus feedforward controller and proposed controller in the simulation and experimental results verify the validity of the proposed control scheme.

Appendix A
The values of system parameters

The system parameters are shown in the following equations as in [1]:

$$a_1 = -\frac{R_{C_f} I_{L_m}}{n L_f} \tag{21}$$

$$a_2 = -\frac{I_{L_m}}{n C_f L_f} - \frac{n(I_{L_m} L_m R_{C_f} - C_{in} D_1 R_{C_f} R_{pv} V_{C_{in}})}{C_{in} L_f L_m R_{pv} n^2} - \frac{C_{in} D_1 I_{L_f} R_{C_f}^2 R_{pv} - C_{in} D_1 R_{C_f} R_{pv} V_{C_f}}{C_{in} L_f L_m R_{pv} n^2} \tag{22}$$

0278-0046 (c) 2015 IEEE. Personal use is permitted, but republication/redistribution requires IEEE permission. See http://www.ieee.org/publications_standards/publications/rights/index.html for more information.

This article has been accepted for publication in a future issue of this journal, but has not been fully edited. Content may change prior to final publication. Citation information: DOI 10.1109/TIE.2015.2477484, IEEE Transactions on Industrial Electronics

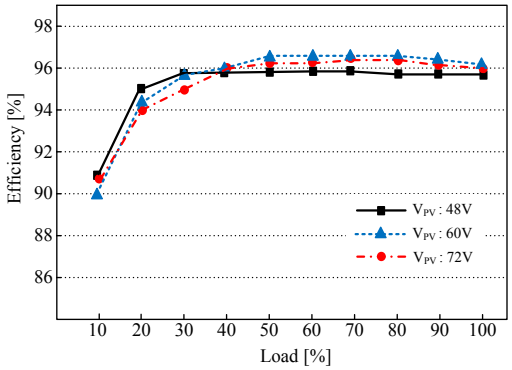

Fig. 10. Measured experimental results for different load conditions.

$$a_3 = \frac{n(-C_f I_{L_m} R_{C_f} R_{pv} D^2 - C_f D_1 I_{L_m} R_{C_f} R_{pv} D - I_{L_m} L_m)}{C_f C_{in} L_f L_m R_{pv} n^2} + \frac{n(-C_f D_1 R_{C_f} V_{C_{in}} + C_{in} D_1 R_{pv} V_{C_{in}})}{C_f C_{in} L_f L_m R_{pv} n^2} + \frac{C_f D_1 R_{C_f} V_{C_f} + C_{in} D_1 R_{pv} V_{C_f} - C_f D_1 I_{L_f} R_{C_f}^2}{C_{in} L_f L_m R_{pv} n^2} - \frac{C_{in} D_1 I_{L_f} R_{C_f} R_{pv}}{C_{in} L_f L_m R_{pv} n^2} \quad (23)$$

$$a_4 = -\frac{n(-D_1 V_{C_{in}} + D^2 I_{L_m} R_{pv} + D_1 D I_{L_m} R_{pv})}{C_f C_{in} L_f L_m R_{pv} n^2} + \frac{D_1 V_{C_f} - D_1 I_{L_f} R_{C_f}}{C_f C_{in} L_f L_m R_{pv} n^2} \quad (24)$$

$$b_1 = \frac{R_{C_f} + R_f}{L_f} + \frac{1}{C_{in} R_{pv}} + \frac{D_1 R_{C_f}}{L_m n^2} \quad (25)$$

$$b_2 = \frac{1}{C_f L_f} + \frac{D^2}{C_{in} L_m} + \frac{(R_{C_f} + R_f)(\frac{1}{C_{in} R_{pv}} + \frac{D_1 R_{C_f}}{L_m n^2})}{L_f} + \frac{D_1^2}{C_f L_m n^2} - \frac{D_1^2 R_{C_f}^2}{L_f L_m n^2} + \frac{D_1 R_{C_f}}{C_{in} L_m R_{pv} n^2} \quad (26)$$

$$b_3 = \frac{(L_m + C_f D^2 R_{C_f} R_{pv} + C_f D^2 R_f R_{pv}) n^2 + D_1^2 L_f}{C_f C_{in} L_f L_m R_{pv} n^2} + \frac{C_f D_1 R_{C_f}^2 - C_f D_1^2 R_{C_f}^2}{C_f C_{in} L_f L_m R_{pv} n^2} + \frac{C_f D_1 R_{C_f} R_f + C_{in} D_1 R_{C_f} R_{pv} - C_f D_1^2 R_{C_f} R_{pv}}{C_f C_{in} L_f L_m R_{pv} n^2} - \frac{C_{in} D_1^2 R_f R_{pv}}{C_f C_{in} L_f L_m R_{pv} n^2} \quad (27)$$

$$b_4 = \frac{D_1^2 R_f - D_1^2 R_{C_f} + D_1 R_{C_f} + D^2 R_{pv} n^2}{C_f C_{in} L_f L_m R_{pv} n^2} \quad (28)$$

$$e_1 = a_1 T_s + a_2 T_s^2 + a_3 T_s^3 + a_4 \quad (29)$$

$$e_2 = -3a_1 T_s - 2a_2 T_s^2 - a_3 T_s^3 \quad (30)$$

$$e_3 = 3a_1 T_s + a_2 T_s^2 \quad (31)$$

$$e_4 = -a_1 T_s \quad (32)$$

$$f_1 = 1 + b_1 T_s + b_2 T_s^2 + b_3 T_s^3 + b_4 T_s^4 \quad (33)$$

$$f_2 = -4 - 3b_1 T_s - 2b_2 T_s^2 - b_3 T_s^3 \quad (34)$$

$$f_3 = 6 + 3b_1 T_s + b_2 T_s^2 \quad (35)$$

$$f_4 = -4 - b_1 T_s \quad (36)$$

where D_1 denotes $1 - D$.

APPENDIX B
DERIVATIONS FOR $G(z)$ AND $S(z)$

Appendix provides the details of derivations for the transfer function from reference to output $G(z)$ and sensitivity function $S(z)$. First, the transfer function from reference to output $G(z)$ is to be derived. From Fig. 5, the following relationship can be obtained

$$y(z) = e(z)\left(1 + k_r \frac{Q(z)z^{-N}}{1 - Q(z)z^{-N}} G_{inv}(z)\right) C_{fb}(z) G_{id}(z), \quad (37)$$

$$e(z) = y_d(z) - y(z). \quad (38)$$

Substituting (38) to (37) and moving y(z)-related term to the left-hand side of (37), we have

$$y(z)\left(1 + \left(1 + k_r \frac{Q(z)z^{-N}}{1 - Q(z)z^{-N}} G_{inv}(z)\right) C_{fb}(z) G_{id}(z)\right) = y_d(z)\left(1 + k_r \frac{Q(z)z^{-N}}{1 - Q(z)z^{-N}} G_{inv}(z)\right) C_{fb}(z) G_{id}(z). \quad (39)$$

Multiplying $1 - Q(z)z^{-N}$ on the both side of (39) and substituting (13) to (39), we obtain

$$y(z)(1 - Q(z)z^{-N} + (1 - Q(z)z^{-N} + k_r z^m Q(z)z^{-N}) \cdot C_{fb}(z) G_{id}(z)) = y_d(z)\left(1 - Q(z)z^{-N} + k_r z^m Q(z)z^{-N}\right) C_{fb}(z) G_{id}(z). \quad (40)$$

Rearranging (40), we have

$$\begin{aligned} G(z) &= \frac{y(z)}{y_d(z)} \\ &= \frac{(1 - Q(z)z^{-N} + k_r z^m Q(z)z^{-N}) C_{fb}(z) G_{id}(z)}{1 - Q(z)z^{-N} + (1 - Q(z)z^{-N} + k_r z^m Q(z)z^{-N}) C_{fb}(z) G_{id}(z)} \\ &= \frac{(1 - Q(z)z^{-N}(1 - k_r z^m)) C_{fb}(z) G_{id}(z)}{1 + C_{fb}(z) G_{id}(z) - Q(z)z^{-N}(1 + C_{fb}(z) G_{id}(z) - k_r z^m C_{fb}(z) G_{id}(z))} \\ &= \frac{1 - Q(z)z^{-N}(1 - k_r z^m)\left(\frac{C_{fb}(z) G_{id}(z)}{1 + C_{fb}(z) G_{id}(z)}\right)}{1 - Q(z)z^{-N}\left(1 - k_r z^m \frac{C_{fb}(z) G_{id}(z)}{1 + C_{fb}(z) G_{id}(z)}\right)} \\ &= \frac{1 - Q(z)z^{-N}(1 - k_r z^m) G_c(z)}{1 - Q(z)z^{-N}(1 - k_r z^m G_c(z))}. \end{aligned} \quad (41)$$

Sensitivity function $S(z)$ can be derived in the same manner of the derivation for $G(z)$. From Fig. 5, the following relationship can also be obtained

$$y(z) = e(z)\left(1 + k_r \frac{Q(z)z^{-N}}{1 - Q(z)z^{-N}} G_{inv}(z)\right) C_{fb}(z) G_{id}(z) + v(z), \quad (42)$$

$$e(z) = -y(z), \quad (43)$$

Substituting (43) to (42) and moving y(z)-related term to the left-hand side of (37), we have

0278-0046 (c) 2015 IEEE. Personal use is permitted, but republication/redistribution requires IEEE permission. See http://www.ieee.org/publications_standards/publications/rights/index.html for more information.

This article has been accepted for publication in a future issue of this journal, but has not been fully edited. Content may change prior to final publication. Citation information: DOI 10.1109/TIE.2015.2477484, IEEE Transactions on Industrial Electronics

$$y(z)\left(1+\left(1+k_r\frac{Q(z)z^{-N}}{1-Q(z)z^{-N}}G_{inv}(z)\right)C_{fb}(z)G_{id}(z)\right) = v(z). \quad (44)$$

Multiplying $1-Q(z)z^{-N}$ on the both side of (44) and substituting (13) to (44), we obtain

$$y(z)(1-Q(z)z^{-N}+\left(1-Q(z)z^{-N}+k_rQ(z)z^{-N}z^m\right) \cdot C_{fb}(z)G_{id}(z)) = (1-Q(z)z^{-N})v(z). \quad (45)$$

Rearranging (45), we have

$$\begin{aligned} S(z) &= \frac{y(z)}{v(z)} \\ &= \frac{(1-Q(z)z^{-N})}{1-Q(z)z^{-N}+(1-Q(z)z^{-N} \\ &\quad + k_rQ(z)z^{-N}z^m)C_{fb}(z)G_{id}(z)} \\ &= \frac{(1-Q(z)z^{-N})}{1+C_{fb}(z)G_{id}(z)-Q(z)z^{-N}(1+C_{fb}(z)G_{id}(z) \\ &\quad - k_rz^mC_{fb}(z)G_{id}(z))} \\ &= \frac{(1-Q(z)z^{-N})(\frac{1}{1+C_{fb}(z)G_{id}(z)})}{1-Q(z)z^{-N}(1-k_rz^m\frac{C_{fb}(z)G_{id}(z)}{1+C_{fb}(z)G_{id}(z)})} \\ &= \frac{(1-Q(z)z^{-N})(1-G_c(z))}{1-Q(z)z^{-N}(1-k_rz^mG_c(z))}. \end{aligned} \quad (46)$$

Finally, $G(z)$ and $S(z)$ can be obtained from (41) and (46).

REFERENCES

[1] F. F. Edwin, W. Xiao, and V. Khankikar, "Dynamic modeling and control of interleaved flyback module-integrated converter for PV power applications," *IEEE Trans. Ind. Electron.*, vol. 61, no. 3, pp. 1377-1388, Mar. 2014.

[2] S. B. Kjaer, J. K. Pedersen, and F. Blaabjerg, "A review of single-phase grid-connected inverters for photovoltaic modules," *IEEE Trans. Ind. Appl.*, vol. 41, no. 5, pp. 1292-1306, Sep./Oct. 2005.

[3] Y. H. Kim, J. W. Jang, S. C. Shin, and C. Y. Won, "Weighted-efficiency enhancement control for photovoltaic AC module interleaved flyback inverter using a synchronous rectifier," *IEEE Trans. Power Electron.*, vol. 29, no. 12, pp. 6481-6493, Dec. 2014.

[4] G. Petrone, G. Spagnuolo, and M. Vitelli, "An analog technique for distributed MPPT PV applications," *IEEE Trans. Ind. Electron.*, vol. 59, no. 12, pp. 4713-4722, Dec. 2012.

[5] Y. Li and R. Oruganti, "A flyback-CCM inverter scheme for photovoltaic AC module application," in Proc. Australasian Univ. Power Eng. Conf. (AUPEC), 2008, pp 1-6.

[6] N. Kasa, T. Iida, and L. Chen, "Flyback inverter controlled by sensorless current MPPT for photovoltaic power system," *IEEE Trans. Ind. Electron.*, vol. 52, no. 4, pp. 1145-1152, Aug. 2005.

[7] N. Sukesh, M. Pahlevaninezhad, and P. K. Jain, "Analysis and implementation of a single-stage flyback PV microinverter with soft switching," *IEEE Trans. Ind. Electron.*, vol. 61, no. 4, pp. 1819-1833, Apr. 2014.

[8] Z. Zhang, X. F. He, and Y. F. Liu, "An optimal control method for photovoltaic grid-tide-interleaved flyback microinverters to achieve high efficiency in wide load range," *IEEE Trans. Power Electron.*, vol. 28, no. 11, pp. 5074-5087, Nov. 2013.

[9] H. Hu, S. Harb, N. H. Kutkut, Z. J. Shen, and I. Batarseh, "A single-stage microinverter without using electrolytic capacitors," *IEEE Trans. Power Electron.*, vol. 28, no. 6, pp. 2677-2687, Jun. 2013.

[10] R. W. Erickson and D. Maksimovic, "Fundamentals of Power electronics," Springer Science & Business Media, 2007.

[11] Y. Li and R. Oruganti, "A low cost flyback CCM inverter for AC module application," *IEEE Trans. Power Electron.*, vol. 27, no. 3, pp. 1295-1303, Mar. 2012.

[12] Y. H. Kim, Y. H. Ji, J. G. Kim, Y. C. Jung, and C. Y. Won, "A new control strategy for improving weighted efficiency in photovoltaic AC module-type interleaved flyback inverters," *IEEE Trans. Power Electron.*, vol. 28, no. 6, pp. 2688-2699, Jun. 2013.

[13] T. V. Thang, N. M. Thao, J. H. Jang, and J. H. Park, "Analysis and design of grid-connected photovoltaic systems with multiple-integrated converters and a pseudo-DC-link inverter," *IEEE Trans. Ind. Electron.*, vol. 61, no. 7, pp. 3377-3386, Jul. 2014.

[14] J. Liu, P. Zanchetta, M. Degano, and E. Lavopa, "Control design and implementation for high performance shunt active filters in aircraft power grids," *IEEE Trans. Ind. Electron.*, vol. 59, no. 9, pp. 3604-3613, 2012.

[15] P. Zanchetta, M. Degano, J. Liu, and P. Mattavelli, "Iterative Learning Control With Variable Sampling Frequency for Current Control of Grid-Connected Converters in Aircraft Power Systems," *IEEE Trans. Ind. Appl.*, vol. 49, no. 4, pp. 1548-1555, 2013.

[16] J. H. Moon, M. N. Lee, and M. J. Chung "Repetitive control for the track-following servo system of an optical disk drive," *IEEE Trans. Control Syst. Technol.*, vol. 6, no. 5, pp. 663-670, 1998.

[17] R. Costa-Castello, J. Nebot, and R. Grino "Demonstration of the internal model principle by digital repetitive control of an educational laboratory plant," *IEEE Trans. Edu.*, vol. 48, no. 1, pp. 73-80, 2005.

[18] S. Chen, Y. M. Lai, S. C. Tan and C. K. Tse"Analysis and design of repetitive controller for harmonic elimination in PWM voltage source inverter systems," *IET Power Electron.*, vol. 1, no. 4, pp. 497-506, 2008.

[19] B. Zhang, D. Wang, K. Zhou, and Y. Wang, "Linear phase lead compensation repetitive control of a CVCF PWM inverter," *IEEE Trans. Ind. Electron.*, vol. 55, no. 4, pp. 1595-1602, 2008.

[20] S. Jiang, D. Cao, Y. Li and F. Z. Peng, "Grid-connected boost-half-bridge photovoltaic microinverter system using repetitive current control and maximum power point tracking," *IEEE Trans. Power Electron.*, vol. 27, no. 11, pp. 4711-4722, 2012.

Sung-Ho Lee was born in Seoul, Korea, in 1985. He received the B.S. degree in electrical engineering from Dongguk University, Seoul, Korea, in 2011. He is currently working toward the Ph.D. degree in electronic and electrical engineering at the Pohang University of Science and Technology, (POSTECH), Pohang, Korea. His research interests include dc-dc converters, grid-connected inverters, renewable energy system, and energy storage system.

Woo-Jun Cha was born in Inchon, Korea, in 1979. He received the M.S. degree in electronic systems engineering from Hanyang University, Ansan, Korea, in 2013. He is currently working toward the Ph.D. degree in electronic and electrical engineering at the Pohang university of Science and Technology (POSTECH), Pohang, Korea. His main research interests include photovoltaic systems, switched-mode power supplies, and advanced LED lighting solutions.

Bong-Hwan Kwon (M'91) was born in Pohang, Korea, in 1958. He received the B.S. degree from Kyungpook National University, Daegu, Korea, in 1982, and the M.S. and Ph.D. degrees from the Korea Advanced Institute of Science and Technology, Seoul, Korea, in 1984 and 1987, respectively all in electrical engineering.

Since 1987, he has been with the Department of Electronic and Electrical Engineering, Pohang University of Science and Technology (POSTECH), Pohang, Korea, where he is currently a Professor. His research interests include converters for renewable energy, high-frequency converters, and switch-mode power supplies.

0278-0046 (c) 2015 IEEE. Personal use is permitted, but republication/redistribution requires IEEE permission. See http://www.ieee.org/publications_standards/publications/rights/index.html for more information.

This article has been accepted for publication in a future issue of this journal, but has not been fully edited. Content may change prior to final publication. Citation information: DOI 10.1109/TIE.2015.2477484, IEEE Transactions on Industrial Electronics

Minsung Kim (M'14) was born in Ulsan, Korea, in 1986. He received the B.S. degree in electrical engineering from Pohang University of Science and Technology (POSTECH), Pohang, Korea, in 2004, and the Ph.D. degree in electrical engineering from POSTECH, Pohang, Korea, in 2013.

Since 2013, he has been with Future IT Research Laboratory, POSTECH, Pohang, Korea, where he is currently senior researcher. His current research interests include renewable energy system, nonlinear system analysis, and controller design for industrial process.

0278-0046 (c) 2015 IEEE. Personal use is permitted, but republication/redistribution requires IEEE permission. See http://www.ieee.org/publications_standards/publications/rights/index.html for more information.